Effects of platform motions on aerodynamic performance and unsteady wake evolution of a floating offshore wind turbine

Hakjin Lee and Duck-Joo Lee*

Korea Advanced Institute of Science and Technology (KAIST), Daejeon 34141, Republic of Korea

Abstract

The capacity of offshore wind power has increased recently because of the emerging environmental and social problems in onshore wind turbines. A floating offshore wind turbine (FOWT) system experiences the additional six-degree-of-freedom (6DoF) motions caused by both wind and wave loads. These motions are associated with the distortion of the wake structure and the oscillation of aerodynamic performance. This study focused on the unsteady wake characteristics of FOWTs. A nonlinear vortex lattice method (NVLM) was coupled with a vortex particle method (VPM) and used for simulation of the NREL 5-MW wind turbine undergoing periodic motions. Translational (heave, sway, and surge) and rotational (yaw, pitch, and roll) motions were imposed on the wind turbine, and the displacements of the floating platform were defined as a sinusoidal function. Significant variations in the thrust force and power output were observed for the streamwise motions. In addition, the platform motions affected the wake evolution strongly, thus resulting in periodic deformation of the wake structure and the rapid breakdown of helical wake vortices for all motions. A discussion of the current study could facilitate in understanding the wake-induced phenomena and the unsteady wake behavior of FOWTs.

Keywords: Floating offshore wind turbine; Six-degree-of-freedom motions; Vortex lattice method; Vortex particle method; Wind turbine wake dynamics

* Corresponding author. KAIST, 291 Daehak-ro, Yuseng-gu, Daejeon 34141, Republic of Korea.
E-mail: djlee@kaist.ac.kr (Duck-Joo Lee)

1. Introduction

According to a statistical study of the demand and installation of wind turbines in Europe, the power capacity of offshore wind turbines has been increasing steadily [1]. Offshore wind technology demonstrates various advantages compared to the bottom-fixed wind turbine onshore or in shallow areas of the sea: (1) Offshore wind is a better quality wind energy resource with high wind speed and uniform wind profile, (2) Concerns of environmental problems, such as noise emission and visual impacts, are less, (3) Potential for constructing a wind farm is higher in regions with a large number of wind turbines in close proximity to each other. Therefore, many researchers have attempted to develop a cost-effective floating offshore wind turbine (FOWT) system to harvest wind energy and reduce the operating and maintenance costs in deep water sites.

FOWTs experience the additional six-degree-of-freedom (6DoF) motions resulting from the platform motions excited by both wind and wave loads. The platform motions cause an asymmetric inflow condition on the rotor blades, leading to significant variations in the aerodynamic performance and fatigue loads. They are also responsible for developing a different wake structure and transient vorticity field compared to bottom-fixed wind turbines. De Vaal et al. [2] investigated the influences of periodic surge motions on aerodynamic loads and induced velocity with various oscillation conditions using blade element momentum (BEM) theory and an actuator disk model. Both numerical models provided similar results in terms of thrust and power coefficients at moderate motion conditions. However, Sebastian and Lackner [3] reported that the BEM theory could yield inaccurate results because the inherent assumptions which are momentum theory and quasi-steady inflow condition can be violated when a wind turbine suffers from platform motions with a large amplitude or fast frequency. In addition, FOWTs may potentially encounter complex flow conditions, such as the vortex ring state or turbulent wake state, owing to severe translational and rotational motions. Therefore, BEM analysis might be inappropriate for analyzing the aerodynamics of FOWTs because it cannot encompass all their operating conditions. To overcome aforementioned limitation of the BEM theory, Sebastian and Lackner utilized a free vortex wake method to simulate a wind turbine experiencing prescribed platform motions [4, 5]. In addition, Jeon et al. [6] and Shen et al. [7] also applied the vortex method to study the unsteady aerodynamics of pitching wind turbines. Tran et al. [8, 9] and Tran and Kim [10] used computational fluid dynamics (CFD) to investigate the unsteady aerodynamic characteristics of the rotor-alone or full-configuration wind turbines experiencing pitch and surge platform motions. The predicted variations in the thrust force and power output were compared with the results of the simplified models, namely the BEM and generalized dynamic wake (GDW) models. Leble and Barakos [11] also conducted unsteady Reynolds-averaged Navier–Stokes (RANS) simulation for computing the aerodynamic performance of wind turbine blades in prescribed yaw and pitch motions. Their results indicated that the motion amplitude and frequency strongly affected the variation in the aerodynamic loads. An experimental study was performed using a scaled down wind turbine model. Rockel et al. [12] measured the flow field behind the wind turbine in the streamwise pitching motion using stereo particle image velocimetry (PIV), and discussed its effects on the mean velocities and their fluctuating components in detail. In previous studies, many researchers primarily focused on predicting the aerodynamic performance of FOWTs without considering the wake dynamics. The unsteady wake behavior of FOWTs and complex wake-induced phenomena have not yet been clearly discussed. From the wind farm perspective, an in-depth understanding of the FOWT wake is required to design a cost-effective floating offshore wind farm; the unsteady wake evolution of the upstream wind turbine can significantly affect the inflow conditions of the downstream wind turbines and leads to negative fluctuating velocity components.

The main aim of the present work is to investigate the effects of the platform motions on the wake evolution as well as the aerodynamic performance of FOWTs. A nonlinear vortex lattice method (NVLM) with vortex particle method (VPM) is adopted to simulate the NREL 5-MW wind turbine model undergoing prescribed platform motions. The unsteady variation in the aerodynamic loads, complex wake structure of FOWTs, and wake-induced phenomena are studied. In particular, the different wake evolving patterns are captured clearly depending on the platform motions, and their impacts on the distribution of axial velocity in the downstream are discussed in detail.

2. Numerical method and wind turbine model

2.1 Aerodynamic model

BEM solvers have been widely used for the comprehensive analysis of wind turbines. A BEM solver is the most computationally efficient aerodynamic model owing to its simple structure; hence, it could be a practical way to design the rotor blade of a wind turbine. However, it might not be suitable for analyzing the aerodynamics of FOWTs because the intrinsic assumption for the momentum theory may be violated when a wind turbine is exposed to large amplitudes or frequencies of motions. Meanwhile, CFD methods can be adopted for the analysis of the floating wind turbine undergoing extreme motions and yield more insightful and accurate solutions. However, they still suffer from unresolved numerical problems such as computationally expensive costs, excessive numerical dissipation errors, and modelling of turbulence. In particular, numerical dissipation errors result in a rapid decay of the wake vortices in the downstream. Hence, CFD methods may fail to describe the unsteady wake behavior, thus leading to an inaccurate load estimation of downstream wind turbines.

In this study, the NVLM is applied to conduct the aerodynamic and wake analyses of the floating wind turbine experiencing periodic platform motions. The primary part of this method is the vortex lattice method (VLM) that is based on the assumption of an incompressible potential flow. Hence, the governing equation becomes the Laplace's equation as a function of velocity potential and its general solution can be represented by distributing the elementary solutions (singular solutions) on the boundaries of the blade surface [13]. Although the VLM can provide reasonably accurate solutions for subsonic flows with affordable computing expense, it cannot intrinsically address the thickness effect, viscous boundary layer effect, and nonlinear aerodynamic characteristics. The NVLM includes an airfoil look-up table and vortex strength correction method to overcome the aforementioned drawbacks of the VLM. First, the rotor blades are modelled by the discrete vortex ring elements in both the chordwise and spanwise directions; further, the linear system of equations are solved to obtain the unknown bound vortex strength on the rotor blades, after which the sectional inflow velocity and effective angle of attack are calculated based on the potential solutions. For the floating wind turbines, the additional velocity component, $\mathbf{V}_{\text{platform}}$, which is given by the sum of the translational ($\mathbf{V}_{\text{trans}}$) and rotational ($\mathbf{V}_{\text{rot}}$) velocities of the FOWT system in Eqs. (1) and (2), are included in the evaluation of the inflow velocity in Eq. (3). Here, $\mathbf{V}_{\infty}$ is the free stream velocity, $\mathbf{\Omega}$ is the rotational velocity of the rotor blade, $\mathbf{r}$ is the position vector, and $\mathbf{V}_{\text{ind,wake}}$ is the induced velocity from the wake vortices. In addition, the inflow velocity is directly associated with the effective angle of attack on the rotor blades in Eq. (4), where β is local twist angle, θ_o is blade pitch angle, $\mathbf{a}_1$ and $\mathbf{a}_3$ are the unit vectors along the tangential and normal to the rotating plane, respectively. Finally, the sectional aerodynamic coefficients can be consulted from the airfoil table as a function of the local inflow velocity and effective angle of attack. In addition, sectional aerodynamic loads are integrated along the span of the rotor blades to estimate the entire performance of the wind turbine including thrust, aerodynamic torque, and power output. Sectional lift forces are used to iteratively correct the bound vortex strength, and the converged bound vortices placed at the trailing edge of the blade will shed into the wake downstream at the next time step. Further details of the present method can be found in previous papers [14, 15, 16] that include the detailed description of the numerical strategies used for the NVLM and validation results.

$$\mathbf{V}_{\text{platform}} = \mathbf{V}_{\text{trans}} + \mathbf{V}_{\text{rot}} \qquad \text{Eq. (1)}$$

$$
\begin{aligned}
\mathbf{V}_{\text{platform}} &= \left(V_{\text{heave}} + \dot{\theta}_{\text{pitch}} z - \dot{\theta}_{\text{roll}} y\right)\hat{\mathbf{i}} \\
&+ \left(V_{\text{sway}} + \dot{\theta}_{\text{roll}} x - \dot{\theta}_{\text{yaw}} z\right)\hat{\mathbf{j}} \\
&+ \left(V_{\text{surge}} + \dot{\theta}_{\text{yaw}} y - \dot{\theta}_{\text{pitch}} x\right)\hat{\mathbf{k}}
\end{aligned} \qquad \text{Eq. (2)}
$$

$$
\mathbf{V}_{\text{inflow}} = \mathbf{V}_{\infty} - \mathbf{\Omega} \times \mathbf{r} + \mathbf{V}_{\text{ind,wake}} + \mathbf{V}_{\text{platform}} \qquad \text{Eq. (3)}
$$

$$
\alpha_{\text{eff}} = \tan^{-1}\left(\frac{\mathbf{V}_{\text{inflow}} \cdot \mathbf{a}_3}{\mathbf{V}_{\text{inflow}} \cdot \mathbf{a}_1}\right) - \left(\beta + \theta_0\right) \qquad \text{Eq. (4)}
$$

2.2 Wake model

A suitable wake model is required to accurately describe the wake development and investigate the wake-induced phenomena. In this study, the wind turbine wake generated from the rotor blade is represented by Lagrangian approach, rather than Eulerian approach. Generally, Eulerian approach suffers from the excessive dissipation error owing to the grid discretization, thus leading to considerable under-prediction in the intensity of tip vortex and a rapid decay of the wake structure in the downstream. It demands high-order numerical schemes with highly dense grid resolution at downstream to accurately capture the vorticity field. In current work, the Lagrangian-based VPM was employed to model the unsteady wake evolution of FOWTs subjected to periodic platform motions. It has been widely used to simulate wind turbine wakes [14-17] and helicopter rotor wakes [18-21]. The major advantage of using this method is that no numerical dissipation error exists because a discretized volume grid is not required for the wake simulation. Therefore, the wake structure can be modelled over a long distance and its effects can be considered though turbulence is not modelled. In addition, the wake structure consisting of vortex particles is allowed to deform freely as the wake evolves downstream. Compared to vortex filaments, vortex particles do not necessarily need to maintain connectivity between adjacent particles. This property is especially useful for investigating the effect of wake interaction. In addition, the unsteady wake behavior and distortion of the wake structure caused by periodic platform motions can be observed with respect to the wake age.

The wind turbine wake was initially developed from the trailing edge along the full span of the rotor blade in the form of trailing and shed vortex filaments, after which they were split into a number of vortex particles. The vorticity fields can be formulated by the sum of the vortex particles as follows.

$$
\boldsymbol{\omega}(\mathbf{x},t) = \sum_{i=1}^{p} \boldsymbol{\alpha}_i(t)\zeta_{\sigma}\left(\mathbf{x} - \mathbf{x}_i(t)\right) \qquad \text{Eq. (5)}
$$

$$\zeta_\sigma(\mathbf{r}) = \frac{1}{\sigma_3}\frac{15}{8\pi}\left[\left(\frac{|\mathbf{r}|}{\sigma}\right)^2 + 1\right]^{-7/2} \qquad \text{Eq. (6)}$$

where p is the total number of vortex particles, $\mathbf{x}$ is the position vector, $\mathbf{r}$ is the position vector between $\mathbf{x}$ and $\mathbf{x}_i$, $\boldsymbol{\alpha}_i(t)$ is the strength vector, σ is the smoothing radius, and $\zeta_\sigma(\mathbf{r})$ is the smoothing function.

The self-induced velocity and mutually induced velocity between the vortex particles must be evaluated at each time step, as in Eqs. (7) and (8). Here, $\mathbf{u}(\mathbf{x}, t)$ is the velocity vector at an arbitrary point ($\mathbf{x}$) in the flow field, $\mathbf{K}_\sigma(\mathbf{r})$ is the regularized Biot–Savart kernel, $q_\sigma(\mathbf{r})$ is the definition of an integration of the smoothing function, and $q(\rho)$ is the three-dimensional high-order algebraic smoothing function [22].

$$\mathbf{u}(\mathbf{x},t) = \sum_{i=1}^{p} \mathbf{K}_\sigma\left(\mathbf{x} - \mathbf{x}_i(t)\right) \times \boldsymbol{\alpha}_i(t) \qquad \text{Eq. (7)}$$

$$\mathbf{K}_\sigma(\mathbf{r}) = -\left(\frac{q_\sigma(\mathbf{r})}{|\mathbf{r}|^3}\right)\mathbf{r}, \quad q_\sigma(\mathbf{r}) = q\left(\frac{|\mathbf{r}|}{\sigma}\right), \quad q(\rho) = \frac{1}{4\pi}\frac{\rho^3\left(\rho^2 + 5/2\right)}{\left(\rho^2+1\right)^{5/2}} \qquad \text{Eq. (8)}$$

In this study, the rotor blades were rotated 5° at each time step (Δψ = 5°) and a numerical simulation was conducted for 15 revolutions to obtain the converged solutions. During the time-marching step, the location of the vortex particles was determined by the second-order Runge–Kutta method as in Eqs. (9) and (10).

$$\mathbf{x}_i(t+\Delta t) = \mathbf{x}_i(t) + \frac{1}{2}\left(k_1 + k_2\right)\Delta t \qquad \text{Eq. (9)}$$

$$k_1 = \mathbf{u}(\mathbf{x}_t,\, t), \;\; k_2 = \mathbf{u}(\mathbf{x}_t + k_1\Delta t,\, t+\Delta t) \qquad \text{Eq. (10)}$$

2.3 Wind turbine model

The NREL 5-MW reference wind turbine model that has been widely used in offshore wind turbine research was considered in the current work. It exhibits a three-bladed upwind configuration with pre-cone and hub tilt angles. The radius of the rotor blade is 63 m and the hub is located 90 m above the bottom-fixed location where periodic platform motions will be imposed. The rotor blade has a tapered-twisted planform and its sectional geometries are composed of a series of Delft University (DU) and NACA airfoils, as listed in Table. 1. The detailed description of the wind turbine model can be found in reference [23]. In the present study, only the three-bladed configuration was considered without the hub, nacelle, tower, and other components, and the blade section comprising only airfoils was represented by the distribution of vortex ring elements in the chordwise and spanwise directions. The grid resolution of each blade was 15 (chordwise) × 30 (spanwise) with a fine distribution in close proximity to the hub and tip regions for capturing the large gradient of the aerodynamic loads and vorticity.

Table 1. Description of NREL 5-MW wind turbine model

Parameter	Value
Rotor configuration	Upwind
Number of blades	3
Rotor radius	63 m
Hub height	90 m
Hub tilt angle	5°
Blade cone angle	2.5°
Blade planform	Tapered-twisted blade
Blade sectional profiles	DU and NACA series airfoils

3. Results and discussion

3.1 Bottom-fixed wind turbine

Prior to conducting the study on FOWTs, the numerical simulation of the NREL 5-MW wind turbine model installed on the fixed foundation was performed for a range of operating conditions. The wind turbine was exposed to below- and above-rated wind speeds at the corresponding rotor speeds and pitch angles, as listed in Table. 2. The rotor speed was regulated to track the optimal tip speed ratio in the below-rated wind condition, while an additional blade pitch angle was applied to maintain the rated power output in the above-rated wind condition. In the present work, the wind turbine model was subjected to below-rated conditions and the profile of the wind speed was assumed to be uniform with respect to the height. To validate the accuracy of the present numerical models, the aerodynamic performance was compared with the reported results in the previously published papers [23, 25], where the BEM and RANS methods were used to estimate the thrust force and power generation of the NREL 5-MW wind turbine model. Fig. 1 shows the variation in the thrust force and power output with respect to the wind speeds. Although a slight disparity exists between the NVLM and RANS results at the above-rated wind speed, the overall results of the NVLM were in excellent agreement with those of the RANS simulation. As shown, the BEM solver tends to overestimate the thrust force significantly compared to the NVLM and RANS results. The comparison results demonstrated that the present numerical model could accurately predict the aerodynamic performance of wind turbines operating in all wind speed conditions.

Table 2. Rotor speed and blade pitch angles depending on wind speed

Wind speed V_∞ [m/s]	Rotor speed Ω [rpm]	Tip speed ratio λ [-]	Blade pitch angle θ_0 [°]
6	7.92	8.71	0
8	9.16	7.55	0
11	12.1	7.26	0
15	12.1	5.32	10.45
20	12.1	3.99	17.47
25	12.1	3.19	23.47

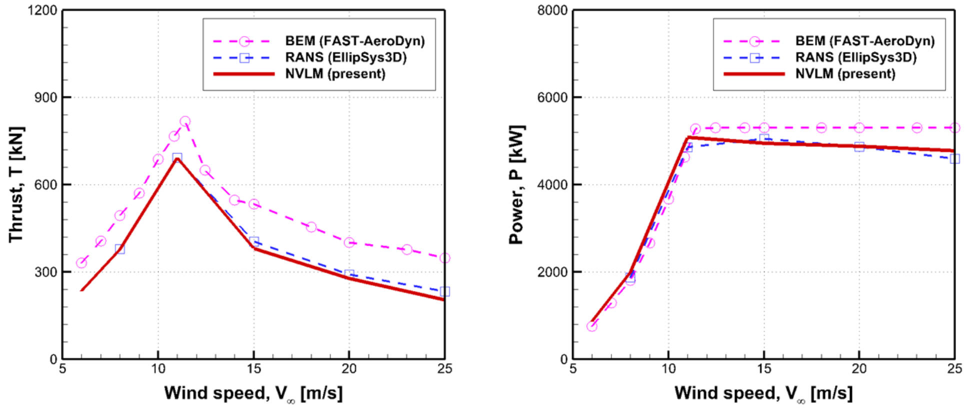

Fig. 1. Comparison of thrust force and power out for bottom-fixed wind turbine

3.2 Floating wind turbine under single-DoF motion

The present paper is a preliminary study on the wake evolution of FOWTs. The wind turbine was forced to move periodically along each axis. Periodic translational (heave, sway and surge) and rotational (yaw, pitch, and roll) platform motions were imposed on the bottom-fixed location of wind turbine where it is located 90 m below the hub, as shown in Fig. 2. Firstly, single-DoF motions, rather than combined multiple-DoF motions, were considered. The displacement of the platform motion can be defined using a simple sine function with motion amplitude (A) and frequency (f) in Eq. (11), and as depicted in Fig. 3 where their values are critical in determining the aerodynamic performance and wake evolution of the FOWTs. The amplitude and frequency of single-DoF platform motions were consulted from previous studies [8, 10, 24], as listed in Table. 3. However, the conditions used in the previous studies [8, 10] included impractical and unrealistic platform motions that might lead to excessive boundary layer separation from the rotor blades. The amplitudes and frequencies for translational and rotational motions were defined to satisfy the following two conditions: (1) The distribution of the effective angle of attack in the radial direction does not exceed the stall-onset angle of attack, (2) The velocity magnitude induced by the translational and rotational motions at the hub height should be of similar value, and this is the reason why the frequency of rotational motion is less than that of translational motion. These motion conditions with below-rated wind speed ensure that the boundary layer separation from the suction side of the rotor blade will not occur. Blade stall is of little concern in this study. Therefore, a pitch control algorithm was not adopted.

$$x(t) = A \sin(2\pi f t) \qquad \text{Eq. (11)}$$

Table 3. Amplitude and frequency of prescribed single-DoF motions

Motion	Amplitude A [m or °]	Frequency f [Hz]
Translation (heave, sway, surge)	4	0.1
Rotation (yaw, pitch, roll)	4	0.05

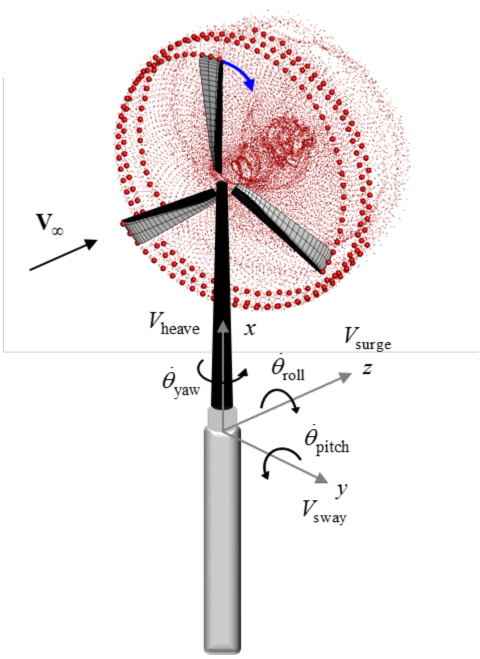

Fig. 2. Six-degree-of-freedom motions of a floating offshore wind turbine system

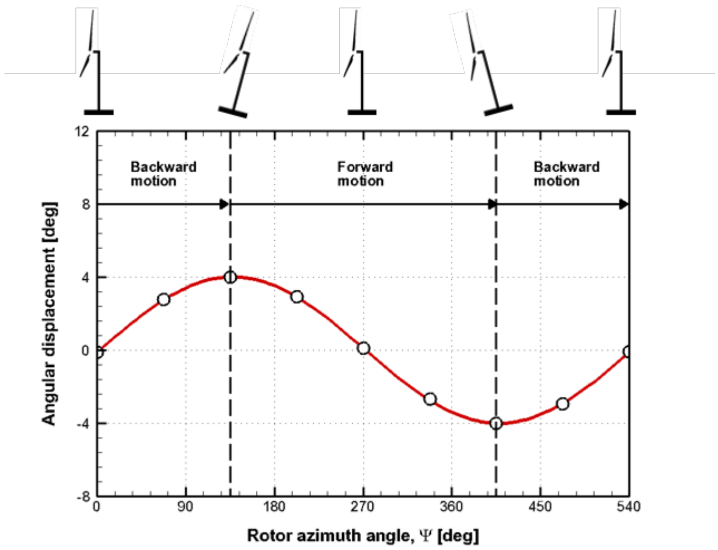

Fig. 3. Periodic pitching motion (A = 4°, f = 0.1 Hz)

The wind turbine was subjected to the incoming wind speed of 8 m/s and rotor speed of 9.16 rpm. The aerodynamic performance of the NREL 5-MW wind turbine model under periodic platform motions was compared with those of the bottom-fixed motions. Figs. 4 and 5 show the variation in the thrust force and power output of the wind turbine undergoing translational and rotational motions, respectively. It is apparent that the surge and pitch motions lead to sinusoidal variation in the aerodynamic performance of the wind turbine, while the heave, sway, yaw, and roll motions had little effect on them. In addition, the frequencies of the variation in the thrust force and power output are consistent with the frequencies of the platform motions. The effects of the surge and pitch motions on the thrust and power output can be verified clearly against the results of other motions and fixed wind turbine performance.

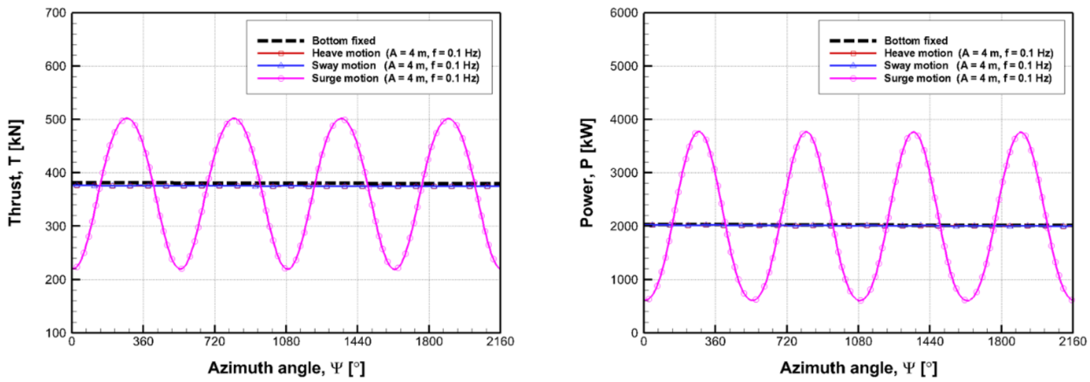

Fig. 4. Variation in the thrust and power of wind turbine in translational motions (A = 4 m, f = 0.1 Hz)

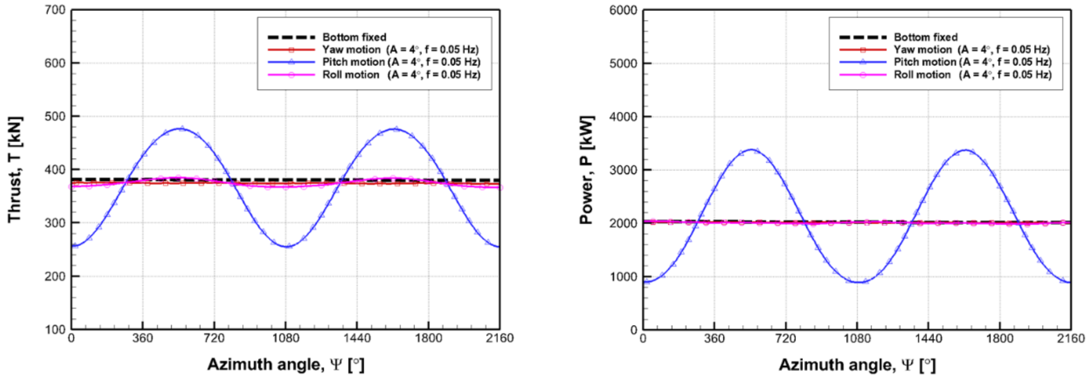

Fig. 5. Variation in the thrust and power of wind turbine in rotational motions (A = 4 °, *f* = 0.05 Hz)

Figs. 6–9 show the comparison between the maximum and minimum values of the aerodynamic performance of the wind turbine under surge and pitch motions with different motion amplitudes. For the motion frequency of 0.03 Hz, the amplitudes of the translational and rotational motions were changed from 4 to 12 m and 2 to 6°, respectively. It appeared that the differences between the maximum and minimum values tend to increase gradually as the motion amplitude increases. In particular, the peak magnitudes of the power output were influenced more significantly by the periodic streamwise motions, resulting in varying the peak values from 17.82 to 58.64 %. Meanwhile, the relative percentage difference in the peak magnitudes of the thrust forces varied approximately from 7.16 to 28.46 %. This appears to be proportional to the power law dependency with inflow speed. It indicated that the streamwise motions could cause severe aerodynamic loads acting on the rotor blades even in the case of a relatively low oscillating frequency.

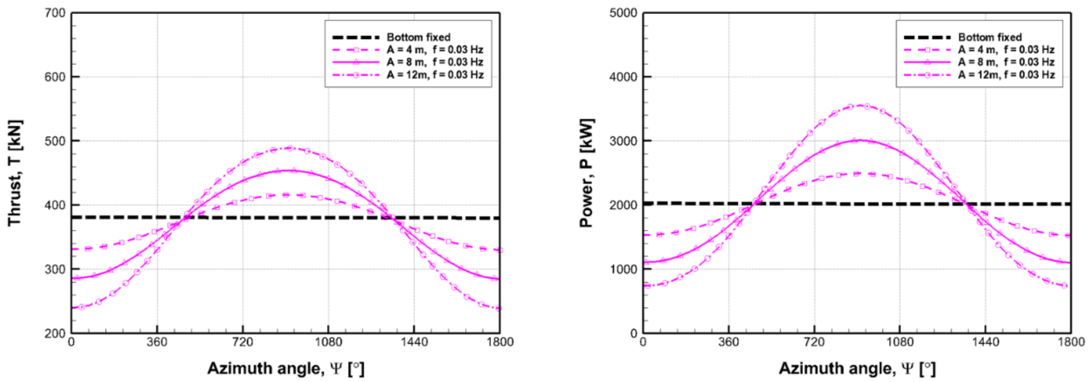

Fig. 6. Variation in the thrust and power of wind turbine in the surge motions (*f* = 0.03 Hz)

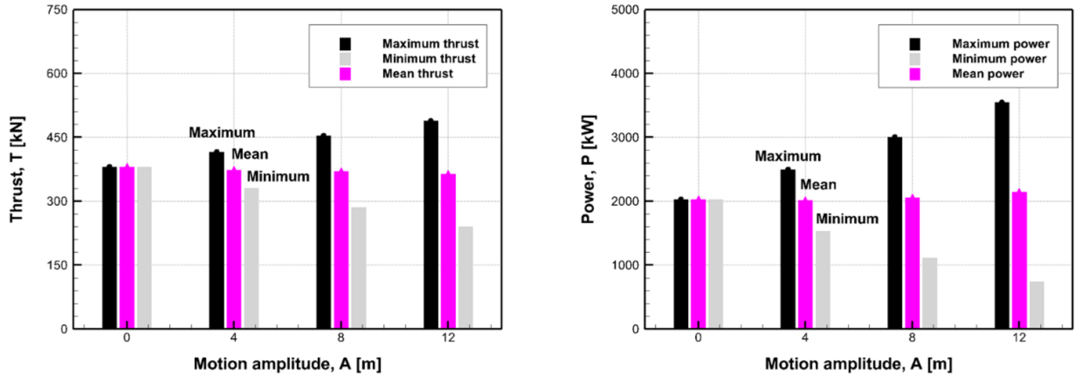

Fig. 7. Maximum, minimum, mean thrust, and power of wind turbine in the surge motions (f = 0.03 Hz)

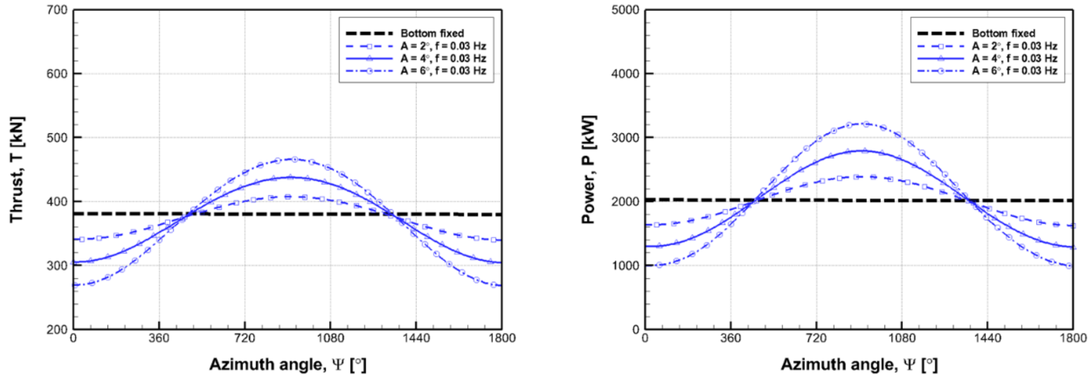

Fig. 8. Variation in the thrust and power of wind turbine in the pitch motions (f = 0.03 Hz)

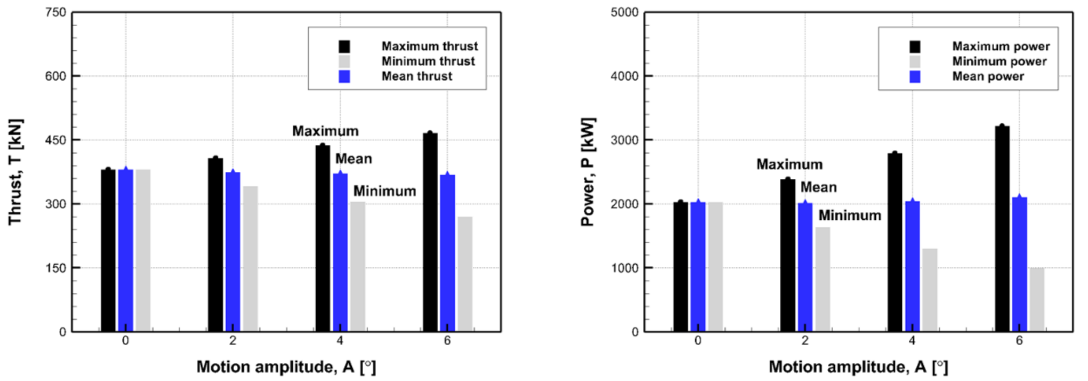

Fig. 9. Maximum, minimum, mean thrust, and power of wind turbine in the pitch motions (f = 0.03 Hz)

In the present study, the wind turbine wake originating from the trailing edge of the rotor blade was modelled by Lagrangian-based vortex particles. They interact with and influence each other mutually during wake convection. The color of vortex particle indicates the wake strength; the particles in red exhibit strong vorticity magnitude, while the green particles exhibit relatively weak vorticity magnitude. Fig. 10 shows the wake structures of non-floating and floating wind turbines as viewed from the side (x-z plane) and above (y-z plane). For the bottom-fixed wind turbine, the wake behind the rotor blades was initially developed in a form of a well-defined helical geometry, as shown in Fig. 10(a). Its structure was preserved over a downstream distance of three times of the rotor diameter and finally evolved into a turbulent wake. The strength of the helical wake vortices was azimuthally symmetric. On the contrary, completely different wake structures evolved and periodic variations in the wake strength with respect to the wake age was clearly manifested for the floating wind turbine. The comparison of Figs. 10 (a)–(g) indicated that the translational and rotational platform motions yielded highly unsteady wake solutions. It is noteworthy that although the aerodynamic performance of the FOWTs was affected significantly by only surge and pitch motions, unsteady and asymmetric wake structures were developed under all motion conditions. The wake vortices were deformed periodically in the up-and-down direction for the heave and yaw motions, side-to-side direction for the sway and roll motions, and forward-and-backward direction for the surge and pitch motions. The wake geometry and strength varied considerably according to the phase of the oscillating wind turbine. The streamwise platform motions, such as the surge and pitch motions, particularly resulted in the most unstable deformation of the wake structures. When the wind turbines moved in the wind direction, the relative velocity between the incoming wind and moving wind turbines decreased, and the effective axial velocity on the rotor blade decreased. These changes resulted in the reduced aerodynamic loads and wake vorticity. On the contrary, when the wind turbines moved in the opposite direction to the incoming wind, aerodynamic loads and wake vorticity increased again. The intermediate wake became highly unstable because of the mutual interaction between the neighboring wake vortices of different strengths. The strong wake-to-wake interaction caused the growth of the wake instability that is related to the tip vortex breakdown phenomenon. Consequently, the wake structures of the wind turbine undergoing platform motions were highly distorted, and the transition into turbulent wake and the destruction of the helical wake structure occurred earlier than the bottom-fixed case. It was apparent that the platform motions highly affected how the wind turbine wake evolves in the downstream, as well as the aerodynamic performance of FOWTs.

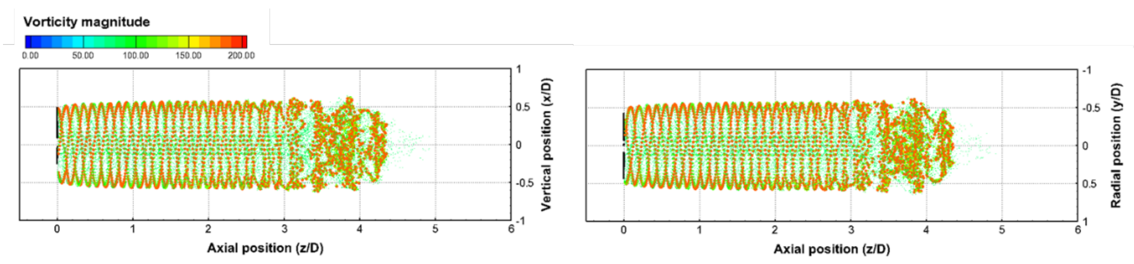

(a) Bottom-fixed wind turbine

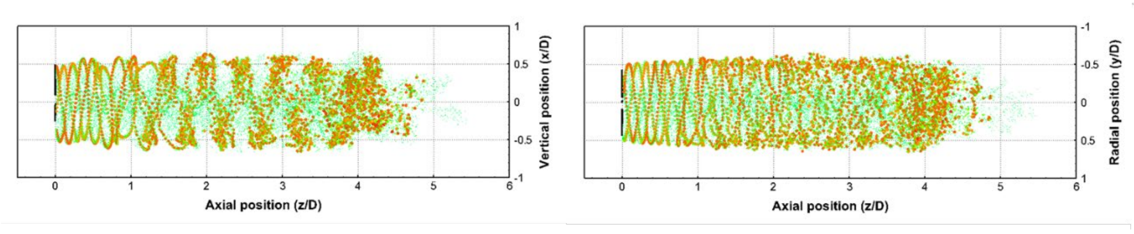

(b) Heave motion

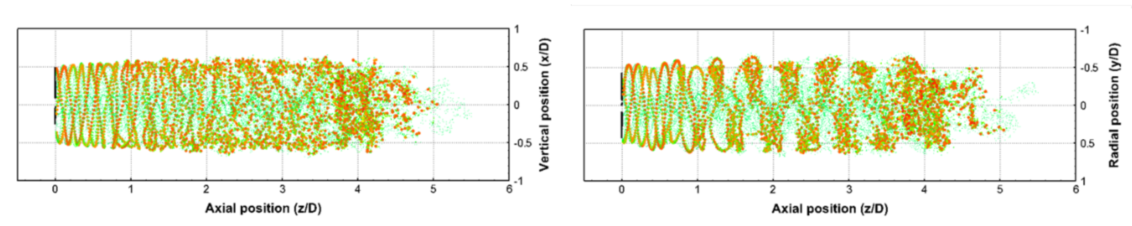

(c) Sway motion

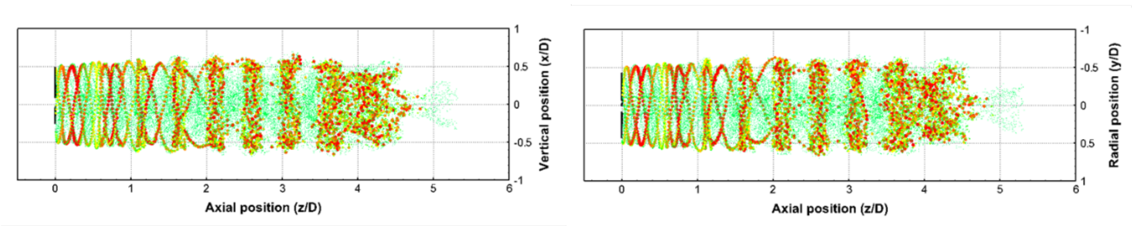

(d) Surge motion

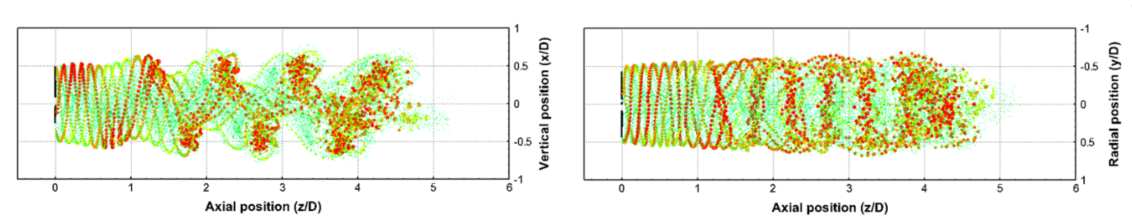

(e) Yaw motion

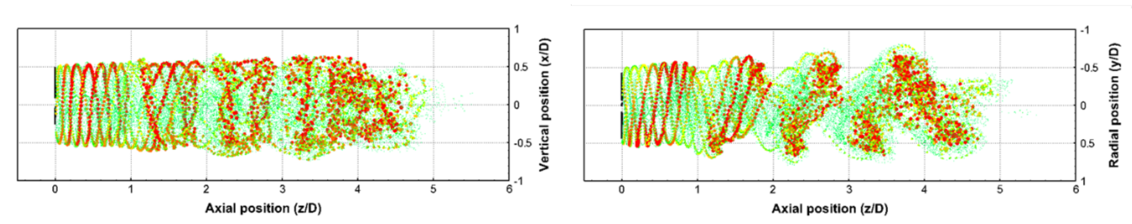

(f) Pitch motion

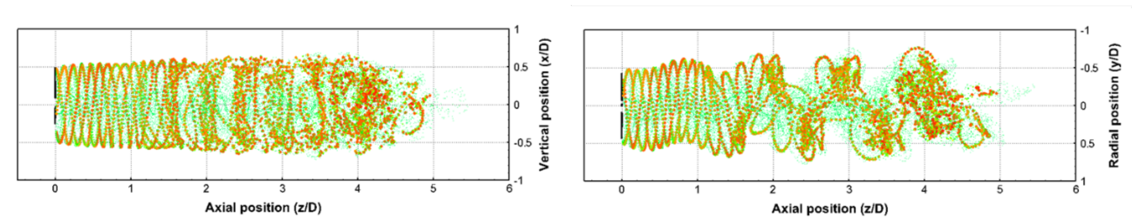

(g) Roll motion

Fig. 10. Wake structure of wind turbine under periodic motions: x-z plane (left) and y-z plane (right)

Wake-induced velocity components yield velocity perturbations in the flow fields behind the rotor blades. To ascertain the influence of the unsteady wake structure of the FOWTs on the velocity field in the downstream, the axial (streamwise) velocity distribution around the rotor area at the hub height was compared with the bottom-fixed case. From the wind farm perspective, the distribution and magnitude of the axial velocity have a direct bearing on the inflow condition of the downstream wind turbines. Since the inflow condition is an important factor in determining the aerodynamic and fatigue loads of the downstream wind turbine. it should be considered to accurately assess the overall power generation of a floating offshore wind farm and to evaluate the fatigue life cycle of the wind turbine components. Figs. 11 and 12 show the three-dimensional wake structure and the axial velocity distribution on the x-y plane at *z/D* = 1, 2, 3, and 4 locations for the bottom-fixed wind turbine. Here, *D* is the rotor diameter. As shown, the wake vortices evolved in the form of a helical geometry with similar strength. Therefore, the flow fields in the downstream appeared to be steady with respect to the wake age in the case where the wake structure was fully developed. Consequently, the distribution of velocity deficit is symmetric and its magnitude depends only on the radial position.

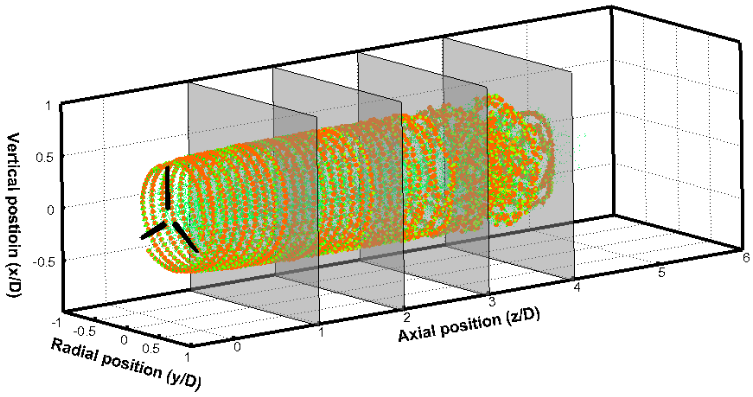

Fig. 11. Three-dimensional wake structure of bottom-fixed wind turbine (t = T)

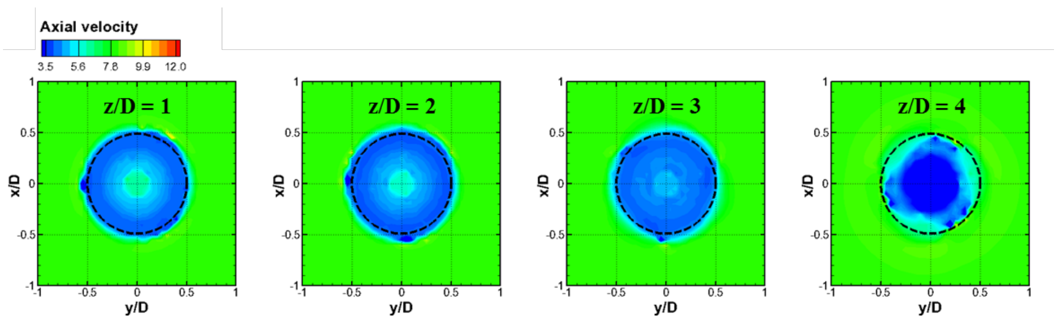

Fig. 12. Axial velocity contours at z/D = 1, 2, 3, and 4: bottom-fixed wind turbine (t = T)

However, the highly deformed wake structure was developed in the case of a wind turbine undergoing pitch motion, as depicted in Fig. 13 where strong and weak vortices were generated periodically owing to the prescribed forward and backward motions in the streamwise direction. Fig. 14 shows the axial velocity contours on the x-y plane at different downstream positions depending on the phase of the wind turbine motion. Here, t is the instantaneous time and T is the period of the platform motion. When the pitch motion occurred, the axial velocity distribution was no longer azimuthally symmetric with respect to the wake age because of the periodically oscillating wake vortices. When strong wake vortices pass through the downstream region, they cause the highly induced velocity in the opposite direction to the incoming velocity, thus leading to low axial velocity in the flow fields. Hence, the floating motions in the streamwise direction affected the distribution and magnitude of the axial velocity component significantly. From a downstream wind turbine perspective, the wind turbines are expected to be exposed to the highly unsteady and asymmetric inflow condition, and their rotor blades will suffer from the highly time-varying aerodynamic loads. Generally, wind turbines require to be installed so that the separation distances between them are approximately 3-10D depending on the prevailing wind directions and the individual circumstances of the wind farm site. Aforementioned, the numerical simulations of floating wind turbine under single-DoF motion were conducted for 15 revolutions with an azimuthal time step of 5°, and the incoming wind speed was 8 m/s. Calculations showed that wind turbine wake can be propagated from the rotor blades to 4.5D downstream. If the numerical simulation was carried out for several more revolutions or at higher wind speed, it could be possible to model the wake propagating father downstream and investigate its impacts in terms of unsteady wake interaction phenomena, asymmetric velocity field, and blade fatigue life cycle of the wind turbine positioned at the downstream.

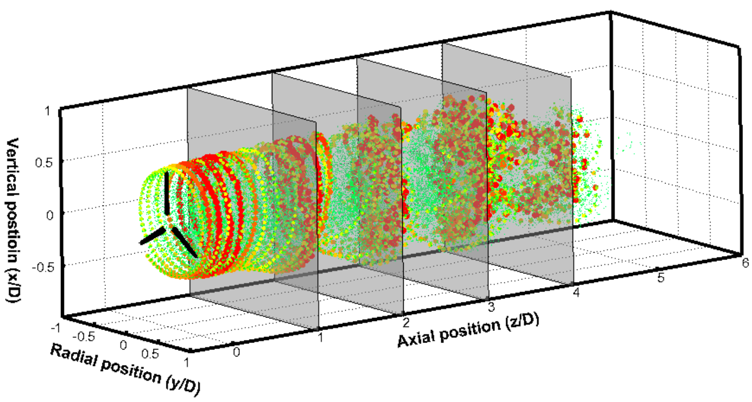

Fig. 13. Three-dimensional wake structure of a floating wind turbine in pitch motion (t = T)

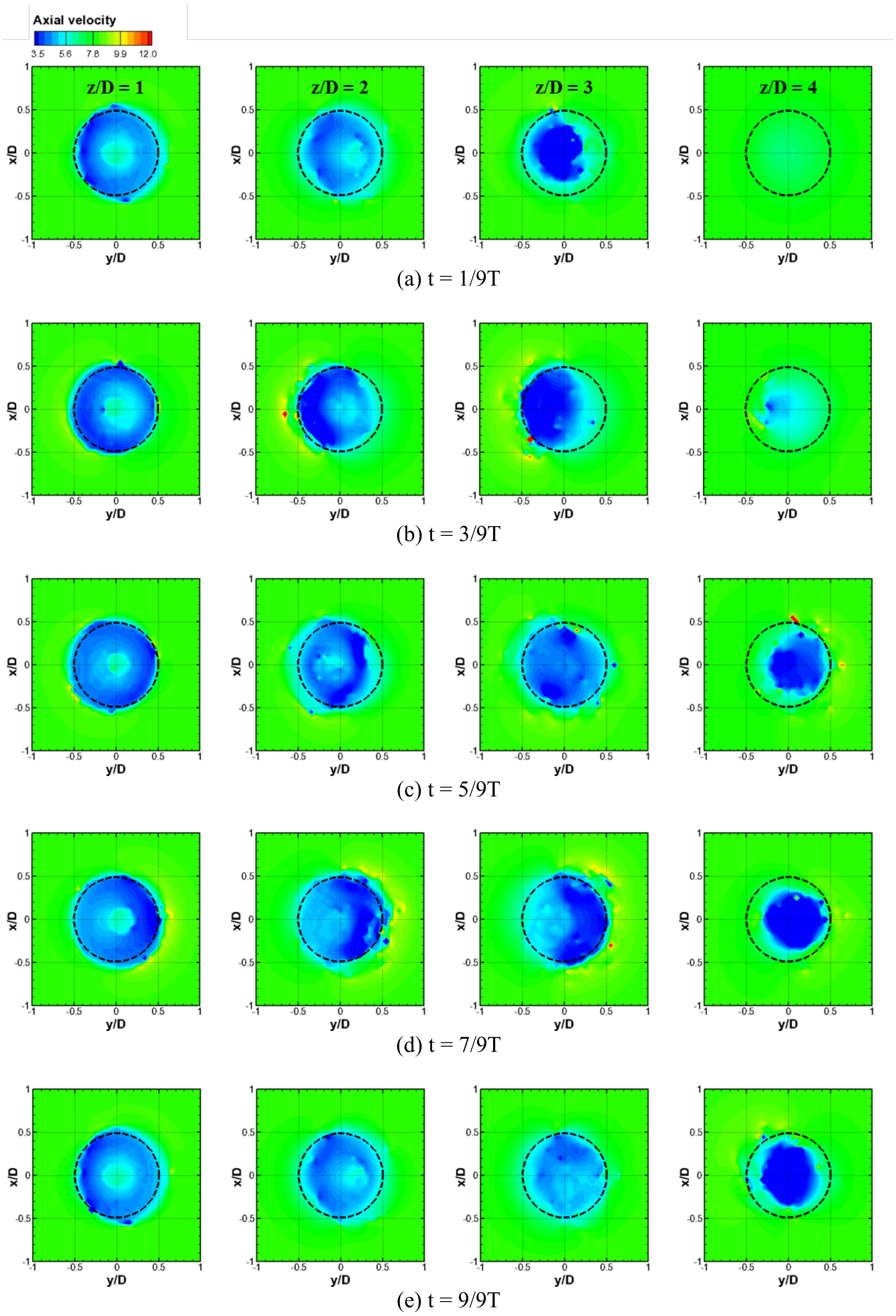

Fig. 14. Axial velocity contours at z/D = 1, 2, 3, and 4: floating wind turbine in pitch motion

3.3 Floating wind turbine under multiple-DoF motion

Generally, large wind turbines of megawatt-class are adopted for the offshore wind turbine system from an economic point of view, and they are typically mounted on three primary floating platforms, namely spar-buoy, tension leg platform (TLP), and barge configurations, as shown in Fig. 15. Herein, three well-known floating platform models that have been used extensively for the fully coupled aerodynamic and hydrodynamic analysis are introduced briefly. The OC3-Hywind spar buoy platform has been suggested from the Offshore Code Comparison Collaboration (OC3) project funded by the International Energy Agency (IEA) Wind Task 23 [26]. This platform is composed of a slender spar buoy, and achieves a static stability using a deep draft combined with ballast weights that shift the center of mass (CM) below the center of buoyancy to provide restoring moments. The platform is also moored by three catenary lines to prevent drifting. The MIT/NREL TLP platform has been developed by the Massachusetts Institute of Technology (MIT) [27]. For supporting wind turbines, the restoring moments are produced through the tension in the mooring-lines and over-buoyant platform structures. High-tension lines running between the substructure and the anchoring structures can effectively mitigate the undesirable response to dynamic excitations imposed by the wind and wave loads, and finally result in a dynamically stiff offshore wind turbine system that could operate like a bottom-fixed wind turbine. The ITI Energy barge platform has been developed by the Universities of Glasgow and Strathclyde [28]. This model features the least expensive and simplest supporting substructure consisting of a large barge platform with eight catenary mooring lines. The large barge-type floating platform with large waterplane area and distributed buoyancy are critical in maintaining the static stability of the combined turbine-platform system. However, the primary drawback of the barge platform is that the floating offshore wind turbine system consisting of a barge platform suffers from much greater platform motions in all modes because of a relatively shallow draft compared to the TLP and spar-buoy systems. The properties of the three floating platforms are detailed in Table 4. Although floating wind turbine with three platform configurations are exposed to the same atmospheric condition and sea state, the dynamic responses to external forces in terms of the dominant mode of platform motions, peak frequencies and amplitudes are different depending on the floating platform concepts because they achieve their static stabilities through different methods mentioned above.

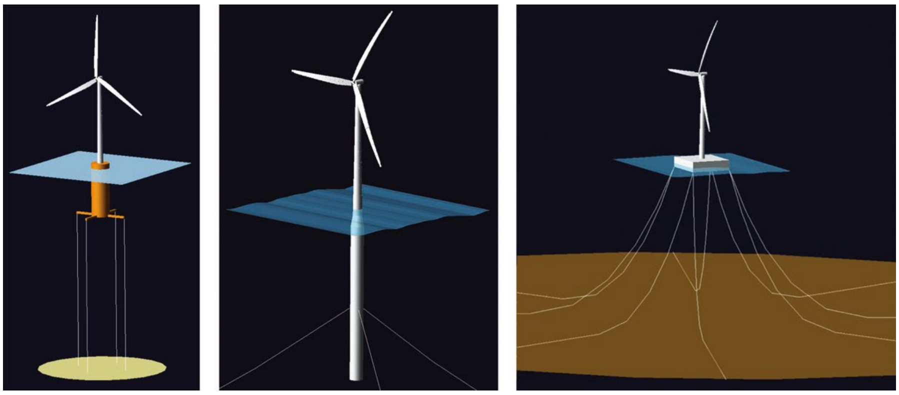

Fig. 15. NREL 5-MW wind turbine with MIT/NREL TLP, OC3-Hywind spar, and ITI Energy barge [28]

Table 4. Description of properties for the three floating platforms [29]

	MIT/NREL TLP	OC3-Hywind spar buoy	ITI Energy barge
Diameter or width × length [m]	18	6.5–9.5	40 × 40
Draft [m]	47.89	120	4
Water depth [m]	200	320	250
Water displacement [m^3]	12,180	8,029	6,000
Mass [10^3 kg]	8600	7466	5452
CM location below SWL [m]	40.61	89.92	0.28
Roll inertia about CM [10^6 kg·m^3]	571.6	4,229	726.9
Pitch inertia about CM [10^6 kg·m^3]	571.6	4,229	726.9
Yaw inertia about CM [10^6 kg·m^3]	361.4	164.2	1,454

Three multiple-DoF simulations were performed to investigate the impacts of multiple-DoF motions on the aerodynamic loads and wake structures. NREL 5-MW reference wind turbines with three concepts of floating platforms were considered. In this work, the fitted floating motions were imposed using a set of synthesized equation, sinusoids of the form given by Eq. (12), rather than applying the actual time series of platform motions to the NVLM simulation because NVLM has not yet been coupled with the hydrodynamics and platform dynamics codes. Eq. (12) indicates that the actual time series are modelled by the linear superposition of two sinusoidal functions as a function of the two peak frequencies of each primary platform mode where two peak frequencies are associated with the sea state and 1P rotor rate. This approach has been proposed by Sebastian and Lackner [30]. They carried out comprehensive analysis for obtaining the simulated time series of platform motions of a floating offshore wind turbines using FAST (Fatigue, Aerodynamics, Structures, and Turbulence) tool, developed by NREL (National Renewable Energy Laboratory). FAST simulations were conducted at a wind speed of 6 m/s, rotor speed of 8.76 rpm, and JONSWAP (The Joint North Sea Wave Project) irregular wave conditions in terms of significant wave height (H_s) of 1.83 m and peak spectral period (T_s) of 12.72 sec. This sea state is defined from the wind and wave data that are provided by ARGOSS (Advisory and Research Group on Geo Observation Systems and Services) [28]. Further details, including operating conditions and settings for the FAST simulation, are addressed in the reference [30]. Sebastian and Lackner's FAST simulations showed that the most dominant modes of platform motions are surge and pitch motions (streamwise motions), while the amplitudes of the sway and roll motions (cross-streamwise motions) are relatively small for all floating platforms. Sebastian and Lackner demonstrated that the primary platform modes, the most significant platform DoF to contribute to variations in angle of attack, can be determined through the power spectral density (PSD) analysis. Therefore, only primary platform modes of each floating structure are used to prescribe the fitted floating motions as listed in Table 5.

$$\vec{x}(t) = \vec{x}_0 + \vec{A}_1 \sin(2\pi \vec{f}_1 t + \vec{\phi}_1) + \vec{A}_2 \sin(2\pi \vec{f}_2 t + \vec{\phi}_2) \quad \text{Eq. (12)}$$

Table 5. Amplitude and frequency of prescribed multiple-DoF motions [30]

Floating platform	Mode	$\vec{x}_0$ [m or °]	$\vec{A}_1$ [m or °]	$\vec{f}_1$ [Hz]	$\vec{\phi}_1$ [rad]	$\vec{A}_2$ [m or °]	$\vec{f}_2$ [Hz]	$\vec{\phi}_2$ [rad]
ITI Energy barge	Heave	-0.130	0.318	0.078	1.303	0.254	0.108	2.702
	Surge	13.602	0.725	0.007	-1.163	-0.442	0.078	2.609
	Pitch	0.591	1.475	0.078	-0.066	1.630	0.083	1.816
OC3-Hywind spar-buoy	Pitch	1.580	-0.084	0.066	1.930	-0.116	0.077	3.113
	Yaw	-0.021	0.091	0.108	1.983	-0.036	0.120	3.429
MIT/NREL TLP	Surge	1.206	0.436	0.016	-0.831	-0.222	0.077	3.018

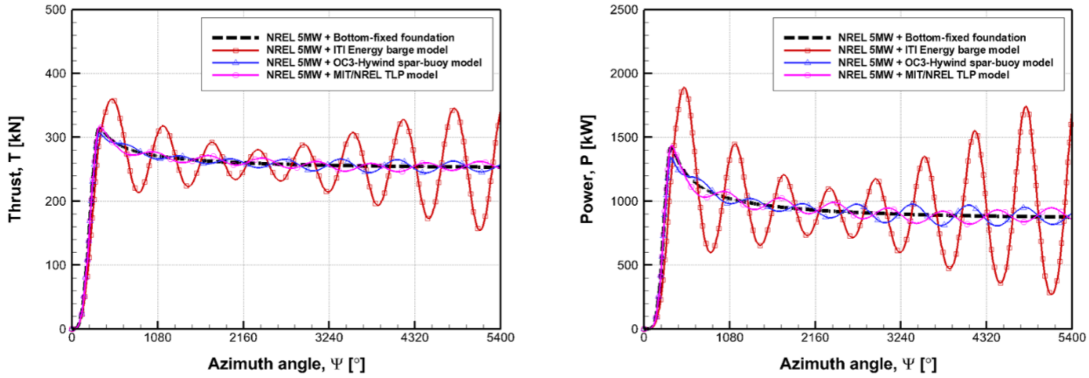

Fig. 16. Variation in the thrust and power of wind turbine in multiple-DoF motions

According to PSD analysis conducted by Sebastian and Lackner, only the aerodynamically significant modes were applied to fit the motion of each platform, i.e. heave, surge, and pitch motions for ITI Energy barge, pitch and yaw motions for OC3-Hywind spar-buoy, and surge motion for MIT/NREL TLP. It is observed that the wind turbine mounted on the barge platform experienced greater platform motions in all modes, particularly in heave, surge, and pitch motions, compared to the spar and TLP platforms. The dynamically excessive motions of barge platform resulted in a significant variation in the aerodynamic loads, and complex wake structures, as shown in Figs. 16 and 17. Meanwhile, the OC3-Hywind spar system exhibits a significantly smaller pitch motion than that of the ITI Energy barge system owing to the deep draft combined with ballast weights. In addition, the MIT/NREL TLP system suffered from only surge motion because the high-tension mooring lines produced restoring moments and high inertia resistance to the rotational motion. This limited platform motion yielded a slight disparity in the wind turbine performance and wake structure between the land-based wind turbine and TLP system. Consequently, it turns out that the spar-buoy and TLP systems are much more stable than barge type of floating structure.

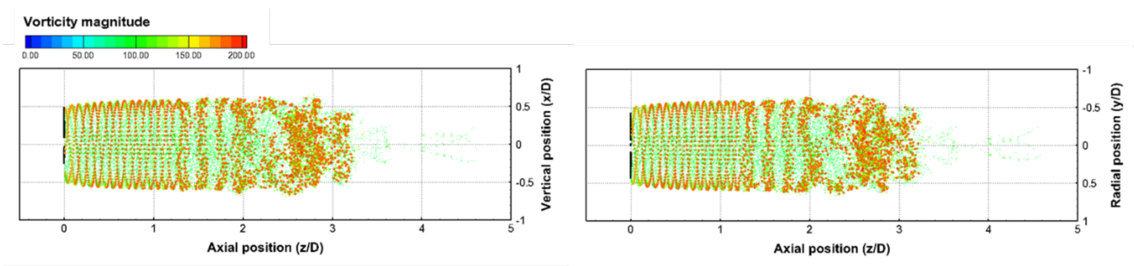

(a) Wind turbine with bottom-fixed foundation

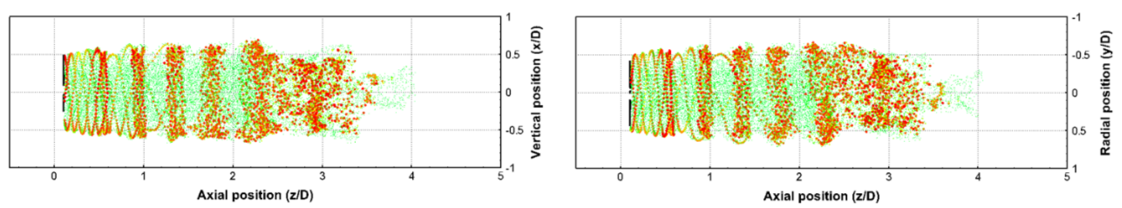

(b) Wind turbine with ITI Energy barge

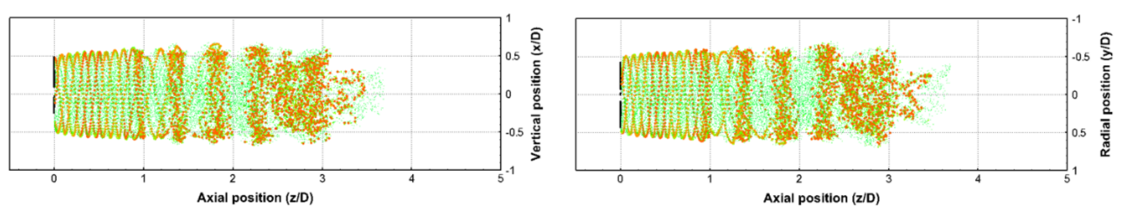

(c) Wind turbine with OC3-Hywind spar-buoy

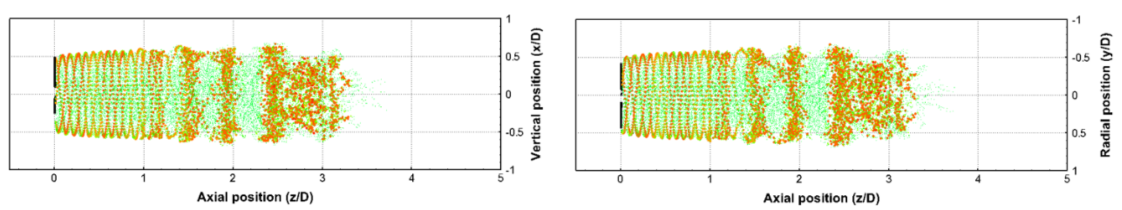

(d) Wind turbine with MIT/NREL TLP

Fig. 17. Wake structures of wind turbine under multiple-DoF motions: x-z plane (left) and y-z plane (right)

4. Conclusion

The main focus of the present study was to investigate the impacts of the platform motions on the wake evolution as well as the aerodynamic performance of FOWTs. The periodic translational (heave, sway, and surge) and rotational (yaw, pitch, and roll) motions in the x, y, and z directions were imposed on the NREL 5-MW wind turbine, and numerical simulations were performed using the NVLM coupled with the VPM. The results were compared with the bottom-fixed case. Calculations for wind turbine undergoing single-DoF motions showed that the only motions in the streamwise direction including surge and pitch motions affected the thrust force and power output of the wind turbine significantly, because the streamwise components of the motion-induced velocities were critical in determining the effective angle of attack. These motions caused a significant oscillation in the aerodynamic performance and oscillation frequency was consistent with the frequency of the platform motions. Meanwhile, periodic deformations of the near and intermediate wake structures with respect to the wake age were observed for all motions. The unsteady wake evolution eventually provoked a rapid breakdown of the helical wake vortices and significant distortion of the far wake in the downstream. Consequently, a significant wake instability appeared and highly unstable wake vortices developed in the floating wind turbine compared to the bottom-fixed turbine. In addition, these changes caused an asymmetric distribution of velocity deficit around the rotor area, thus resulting in unsteady inflow conditions on the wind turbine positioned downstream. Furthermore, numerical simulations of wind turbine with three primary floating platforms including spar-buoy, TLP, and barge configurations were performed to compare how the aerodynamic performance and wake structure vary depending on the type of substructure. Calculations for wind turbines undergoing multiple-DoF motions showed that barge system experienced the most severe platform motions and yielded highly unsteady variation in the wind turbine performance and wake geometry. A discussion of this work could facilitate in better understanding the wake-induced phenomena and evolving pattern of the FOWT wake. This provides a scope for further research to design a more efficient layout of floating wind systems and analyze the unsteady wake dynamics of floating offshore wind farms.

A limitation of the present study is that the rotor blades were assumed to be rigid. Hence, the influences of the blade deflection were not included. A flexible blade introduces structural couplings which might affect different development of wake structure. In addition, NVLM has not yet been coupled with the hydrodynamics and platform dynamics codes. It is more desirable to include aeroelastic and hydrodynamic studies for the comprehensive analysis of FOWTs. Methods for modelling the viscous diffusion effect are also required in vortex particle method to consider viscous effects on wake structure. These are our future works.

Declaration of interest

There is no conflict of interest

Acknowledgments

This work was supported by the Korea Institute of Energy Technology Evaluation and Planning (KETEP) and the Ministry of Trade, Industry & Energy (MOTIE) of the Republic of Korea (No. 20168520021200). This work was also supported by Space Core Technology Development Program through the National Research Foundation of Korea (NRF), which is funded by the Ministry of Science, ICT & Future Planning [NRF-2014M1A3A3A02034837].

References

[1] Fraile, D., Mbistrova, A., Pineda, I., Tardieu, P., and Miró L.,"Wind in power 2017: Annual combined onshore and offshore wind energy statistics," WindEurope, 2018.

[2] De Vaal, J. B., Hansen, M. O. L., and Moan, T., "Effect of wind turbine surge motion on rotor thrust and induced velocity," *Wind Energy*, 17, 2014, pp.105-121.

[3] Sebastian, T., and Lackner, M., "Characterization of the unsteady aerodynamics of offshore floating wind turbines," *Wind Energy*, 16, 2013, pp.339-352.

[4] Sebastian, T., and Lackner, M., "Analysis of the induction and wake evolution of an offshore floating wind turbine," *Energies*, 5, 2012, pp.968-1000.

[5] Sebastian, T., and Lackner, M., "Development of a free vortex method code for offshore floating wind turbines," *Renewable Energy*, 46, 2012, pp.269-275.

[6] Jeon, M., Lee, S., and Lee, S., "Unsteady Aerodynamics of Offshore Floating Wind Turbines in Platform Motion Using Vortex Lattice Method," *Renewable Energy*, 65, 2014, pp.207-212.

[7] X. Shen, P. Hu, J. Chen, X. Zhu, and Z. Du, "The unsteady aerodynamics of floating wind turbine under platform pitch motion," *Proceedings of the Institution of Mechanical Engineers, Part A: Journal of Power and Energy*, 2018. pp.1-18.

[8] Tran, T. T., Kim, D. H., and Song, J. S., "Computational Fluid Dynamic Analysis of a Floating Offshore Wind Turbine Experiencing Platform Pitching Motion," *Energies*, 7, 2014, pp.5011-5026.

[9] Tran, T. T., Kim, D. H., and Nguyen, B. H., "Aerodynamic Interference Effect of Huge Wind Turbine Blades with Periodic Surge Motions Using Overset Grid-Based Computational Fluid Dynamics Approach," *Journal of Solar Energy Engineering*, 137, 2015, pp.061003.

[10] Tran, T. T., and Kim, D. H., "A CFD study into the influence of unsteady aerodynamic interference on wind turbine surge motion," *Renewable Energy*, 90, 2016, pp.204-228.

[11] Leble, V., and Barakos, G., "10-MW Wind Turbine Performance Under Pitching and Yawing Motion," *Journal of Solar Energy Engineering*, 139, 2017, pp.041003.

[12] Rockel, S., Camp, E., Schmidt, J., Peinke, J., Cal, R. B., and Hölling, M., "Experimental Study on Influence of Pitch Motion on the Wake of a Floating Wind Turbine Model," *Energies*, 7, 2014, pp.1954-1985.

[13] Katz, J. and Plotkin, A., "Low-Speed Aerodynamics," Cambridge Univ. Press, Cambridge, England, U.K., 2001.

[14] Lee, H. J. and Lee, D. J., "Numerical investigation of the aerodynamics and wake structures of horizontal axis wind turbines by using nonlinear vortex lattice method," *Renewable Energy*, 132, 2019, pp.1121-1133.

[15] Lee, H. J. and Lee, D. J., "Wake impact on aerodynamic characteristics of horizontal axis wind turbine under yawed flow conditions," *Renewable Energy*, 136, 2019, pp.383-392.

[16] Lee, H. J., Jo, Y. M., and Lee, D. J., "Development of Nonlinear Vortex Lattice Method and Its Application to Aerodynamic Analysis of Wind Turbine," *6th Asian/Austrailian Rotorcraft Forum and Heli Japan*, 2017.

[17] Voutsinas, S. G., Beleiss, M. A., and Rados, K. G., "Investigation of the Yawed Operation of Wind Turbines by means of a Vortex Particle Method," *AGARD Conference Proceedings*, 552, 1995, pp.11.1-11.

[18] Lee, D. J., and Na, S. U., "Numerical simulations of wake structure generated by rotating blades using a time marching, free vortex blob method," European Journal of Mechanics-B/Fluids, 18(1), 1999, pp. 147–159. 429

[19] Jang, J. S., Park, S. H., and Lee, D. J., "Prediction of Fuselage Surface Pressures in Rotor–Fuselage Interactions Using an Integral Solution of Poisson Equation," *Journal of the American Helicopter Society*, 59(4), 2014, pp. 431 1–11. 432

[20] Zhao, J., and He, C., "A viscous vortex particle model for rotor wake and interference analysis," *Journal of the American Helicopter Society*, 55(1), 2010, pp. 012007-012007.

[21] He, C., and Zhao, J., "Modeling Rotor Wake Dynamics with Viscous Vortex Particle Method," *AIAA Journal*, 47(4), 2009, pp. 902–915.

[22] Winckelmans, G. S. and Leonard, A., "Contributions to Vortex Particle Methods for the Computation of Three-Dimensional Incompressible Unsteady Flows," *Journal of Computational Physics*, 109, 1993, pp. 247–273.

[23] Jonkman, J., Butterfield, S., Musial, W., and Scott, G., "Definition of a 5-MW Reference Wind Turbine for Offshore System Development," Technical Report, NREL/TP-500-38060, 2009.

[24] Wayman, E. N., Sclavounos, P. D., Butterfield, S., Jonkman, J., and Musial, W., "Coupled Dynamic Modeling of Floating Wind Turbine Systems," NREL/CP-500-39481, 2006.

[25] Sørensen, N. N., and Johansen, J., "UPWIND, Aerodynamics and aero-elasticity Rotor aerodynamics in atmospheric shear flow," *European Wind Energy Conference & Exhibition*, EWEC 2007.

[26] Jonkman, J. M., "Definition of the floating system for phase IV of OC3," Technical Report, NREL/TP-500-47535, 2009

[27] Matha, D., "Model development and loads analysis of an offshore wind turbine on a tension leg platform, with a comparison to other floating turbine concepts," M.S. Thesis, Endowed Chair of Wind Energy, Universität Stuttgart, Germany, 2009.

[28] Jonkman, J. M., "Dynamics modeling and loads analysis of an offshore floating wind turbine," Technical Report, NREL/TP-500-41958, 2007.

[29] Jonkman J. M., and Matha, D., "Dynamics of offshore floating wind turbines-analysis of three concepts," *Wind Energy*, 14, 2011. pp. 557-569.

[30] T. Sebastian and M. A. Lackner, "Analysis of the Induction and Wake Evolution of an Offshore Floating Wind Turbine," *Energies*, 5, 2012, pp. 968-1000.

[31] T. Sebastian and M. A. Lackner, "Characterization of the unsteady aerodynamics of offshore floating wind turbines," *Wind Energy*, 16, 2013. pp. 339-352.